Wind and Structures, *Vol. 31, No. 1 (2020) 31-41*
DOI: https://doi.org/10.12989/was.2020.31.1.31

Effect of windshields on the aerodynamic performance of a four-box bridge deck

Xi Chen[1] and Elena Dragomirescu*[2]

[1]Power Construction Corporation of China, Chengdu, Republic of China
[2]Department of Civil Engineering, University of Ottawa, 161 Louis Pasteur, Ottawa, K1N 6N5, ON, Canada

(*Received October 18, 2019, Revised May 23, 2020, Accepted June 8, 2020*)

Abstract. A new type of bridge deck section consisting of four-box decks, two side decks for vehicular traffic lanes and two middle decks for railway traffic, has been experimentally investigated for determining its aerodynamic properties. The eight flutter derivatives were determined by the Iterative Least Squares (ILS) method for this new type of four-box deck model, with two windshields of 30 mm and 50 mm height respectively. Wind tunnel experiments were performed for angles of attack α = ±6°, ±4°, ±2° and 0° and Re numbers of 4.85×105 to 6.06×105 and it was found that the four-box deck with the 50 mm windshields had a better aerodynamic performance. Also, the results showed that the installation of the windshields reduced the values of the lift coefficient CL for the negative angles attack in the range of -6° to 0°, but the drag coefficient CD increased in the positive angle of attack range. However, galloping instability was not encountered for the tested reduced wind speeds, of up to 9.8. The aerodynamic force coefficients and the flutter derivatives for the four-box deck model were consistent with the results reported for the Messina triple-box bridge deck, but were different from those reported for the twin-box bridge decks.

Keywords: flutter derivatives; four-box bridge deck; aerodynamic coefficients; wind tunnel tests

1. Introduction

Suspension bridges are slender structures with main spans of up to 2,000 m, which developed through the years reaching complex geometric deck configurations. Improving the aerodynamic properties by adopting new geometric shapes for the bridge decks was recently attempted by numerous researchers, departing from the single-box girder decks and developing to twin-box and multiple-box girders. Due to their stability and efficiency, several twin-box girder bridges have been constructed in recent years, such as: the Yi Sun-Sin Bridge, with a main span of 1,545 m (Lee *et al*. 2012), the Tsing Ma Bridge with a main span of 1,377 m (Ge and Xiang 2009, Xu *et al*. 1997), the Stonecutters Bridge with a main span of 1,018 m (Morgenthal *et al*. 2010, Hui 2013), the Xihoumen Bridge of 1,650 m main span Kwon *et al*. 2011, etc. However, the bridges with twin-box deck sections could not overpass the 2,000 m main span length. Further advances towards three-decks for Messina Bridge (Diana *et al*. 1995, Baldomir *et al*. 2013), Sunda Strait Bridge, Wangsadinata *et al*. 1992 and Gibraltar Strait II Bridge (Lin and Chow 1991) and four-decks for Megane Bridge (Dragomirescu *et al*. 2016, Wang and Dragomirescu 2016) have been made, thus acknowledging the effect of complex deck geometries on aerodynamic performance of bridges; however none of these long-span bridge designs reached the construction phase.

*Corresponding author, Ph.D. Associate Professor
E-mail: elndrag@uottawa.ca

According to Nieto *et al*. (2012) and Meng (2013), the windshield barriers play an important role in the aerodynamic properties of long-span bridge decks, and this element should be an inseparable part for an actual bridge deck or the sectional deck model used in experiments. Long-span bridges, located over the sea straits, thus exposed to higher wind loads, usually need to adopt the strip windshields with large porosity. The height of the windshield barrier is an important factor for protecting the vehicles against high lateral wind loads, however these have a direct effect on the static aerodynamic coefficients and the flutter derivatives of the bridge deck itself. Porcino *et al*. (2008) and Kozmar *et al*. (2012) performed wind tunnel experiments and PIV measurements for investigating the effect of the wind angle of attack on two viaducts with wind shields of porosity factors of 30, 43 and 53 for turbulence intensities of 0%, 3.3% and 17% and they found that the variations in horizontal angle of attack do not affect significantly the flow field characteristics along the deck; however when no barriers are employed, the mean incoming wind flow can produce strong vorticity in the immediate vicinity of the road surface. Buljac *et al*. (2017), showed that for a cables stayed bridges with one box deck, the drag coefficients increase with the decrease of shield porosity and with the increase of its height, when the wind barrier is placed at the windward edge of the deck, however these decks were found more susceptible to torsional flutter. Strukelj *et al*. (2005) analyzed the effect of wind barriers geometry on the wind forces formed on the vehicles crossing a viaduct, while Chen *et al*. (2015) studied the dynamic response and the safety of vehicles under crosswind developed from the wind barriers.

For bridge decks with complex geometric configuration,

http://www.techno-press.com/journals/was&subpage=7 ISSN: 1226-6116 (Print), 1598-6225 (Online)

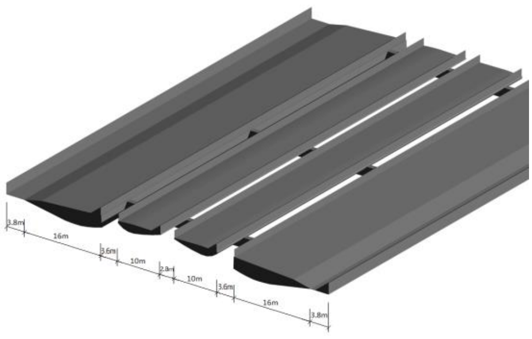

(a)

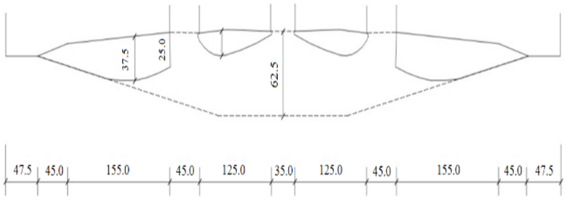

(b)

Fig. 1 (a) Geometric dimensions of the multi-box bridge deck section (mm), (b) Cross-section of the four box bridge deck (mm)

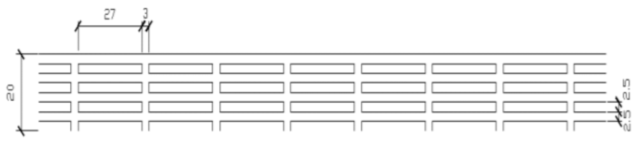

(a)

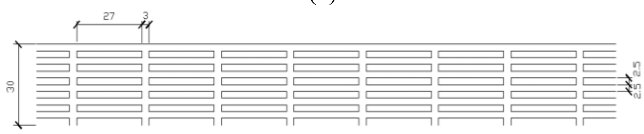

(b)

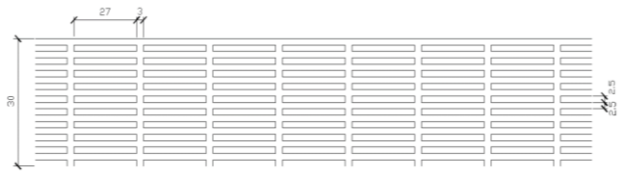

(c)

Fig. 2 Windshields barrier models for (a) 20 mm height windshield for middle decks, (b) 30 mm height wind shield for side decks of Model 1 (c) 50 mm height wind shield for side decks of Model 2

the effect of the windshields on the aerodynamic performance of the bridge might depend on the wind-structure interaction for different angles of attack, among others. The new four-box bridge deck model, consisting of two middle decks for railway and two side decks with sidewalks for traffic and pedestrians has an advanced wind-structure interaction mechanism (Dragomirescu *et al*. 2016), thus it is very important to investigate the effect of the added deck accessories on its aerodynamic performance. In order to finalize the configuration of the four-box bridge deck, the effect of the windshields and median barriers, as additional elements on the bridge deck were used for decreasing the incoming lateral wind, thus preventing the vehicles' rollover and ensuring driving security under high lateral wind force, were investigated for different wind speeds and angles of attack. Therefore wind tunnel tests were performed for wind speeds of 0.8 m/s to 11.0 m/s for angles of attack α = ±6°, ±4°, ±2° and 0°, employing two wind shields models and one type of middle barrier. For the current test, the windshield height was investigated to determine the effect of the wind flow deviated from these windshields, on the aerodynamic properties of the four-box bridge deck section, while the porosity of the windshield was maintained constant.

2. Bridge deck model setup for wind tunnel test

The four-box bridge deck model had a total width of 870 mm, as shown in Figs. 1(a) and 1(b), with the two middle decks of 125 mm width, two traffic decks on both sides of the middle decks of the 200 mm width connected to the two 47.5 mm wide pedestrian/bicycle lanes. The depth of the railway decks and traffic decks were 37.5 mm and 25 mm respectively, with the gap width between the two railway decks of 35 mm. The gap between the railway and traffic decks was 45 mm. Six windshields and barriers of rectangular shape, with 20 mm height and 50% porosity (Fig. 2(a)) were installed on the edges of the middle decks and on the inside edges of the traffic decks, as indicated in Fig. 4; Two windshields of 30 mm height and porosity of 50% (Fig. 2(b)) were installed at the extremities of the bicycle and pedestrian lanes, on the edges of the Model 1; also these were replaceable in order to change the windshield models from the 30 mm high windshield to the 50 mm high windshields (Fig. 2(c)). All the windshields utilized have the same length of 870 mm, spanning the entire bridge deck model and the same barrier cell of 27 mm long and 3 mm high. The four box decks were connected by three stabilizing beams each of 30 mm width and maximum depth of 62.5 mm, installed at 250 mm intervals between the decks.

Four aircraft grade 7075 aluminum sheets of 0.4 cm thickness were attached on the top surfaces of the decks, to eliminate the roughness and also to increase the stiffness of the model. Two aluminum end plates were mounted on each of the extremities of the multiple box bridge deck model, for avoiding the wall effect and for restraining the motion of the individual deck boxes, which would interfere with the overall bridge deck dynamic response (Fig. 3). These were smaller than the usual wood plates used for bridge deck sections, to limit the added weight of the model. The tests were conducted in the open circuit atmospheric boundary layer wind tunnel at Gradient Wind Engineering, which has an overall length of 27 m with a test section of 2.1 m width and 1.8 m height. The maximum testing wind speed in the wind tunnel was 13 m/s; higher wind speeds can be achieved in the wind tunnel, however the experiment was stopped whenever the vertical and torsional vibrations

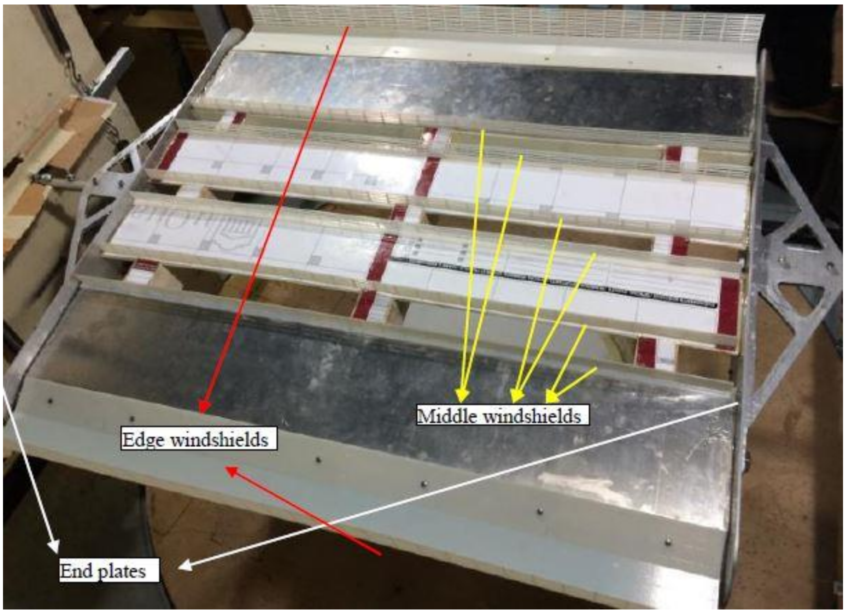

Fig. 3 Four-boxes bridge deck model with windshields

became too aggressive, in order to avoid any permanent damage for the bridge model or of the mounting system.

For the static tests the two longitudinal bars of the bridge deck model were fixed by the aid of steel connecting frames and two custom made force cells were attached at both ends of the longitudinal bar, one for measuring the lift coefficient and the other for measuring the drag coefficient. The force cell measured the strain variation of the steel bar, and the corresponding stresses and forces were determined by using the StrainSmart software. As other wind tunnel studies pointed out (Wang 2015), for multiple box deck, tested for wind speeds higher than 7 m/s, the lift and drag coefficients are not significantly influenced by the increase of the wind speed. Therefore the static tests were performed for wind speeds of 8 m/s to 10 m/s, for angles of attack of -6° to 6°. The corresponding Reynolds numbers are between 4.85×10^5 and 6.06×10^5. The quasi-steady formulation of the wind loads were considered per unit length of deck, as presented by Simiu and Scanlan (1996):

$$D(\alpha) = \frac{1}{2}\rho U^2 B C_D(\alpha) \tag{1}$$

$$L(\alpha) = \frac{1}{2}\rho U^2 B C_L(\alpha) \tag{2}$$

where D and L are the static drag and lift forces, respectively; C_D and C_L are the static drag and lift force coefficients, respectively; ρ is the air density with a value of 1.214 $\mathrm{kg/m^3}$; U is the wind speed; B is the width of the tested bridge deck model, which is 870 mm for the current model.

For the dynamic test, a total of eight springs, with an equivalent elastic constant of k=680 kN/m, were connected to the transversal bar of the bridge deck model, four on the upper side of the model and four on the lower side of the model, as schematically represented in Fig. 4(a). The vertical vibrations of the bridge deck model were measured at both sides of the transversal bar by laser sensors with 5 mm to 35 mm measuring range and 0.01 mm accuracy, each placed at 200 mm from the mid-point of the transverse bar (Fig. 4). The natural frequencies and the damping ratios for

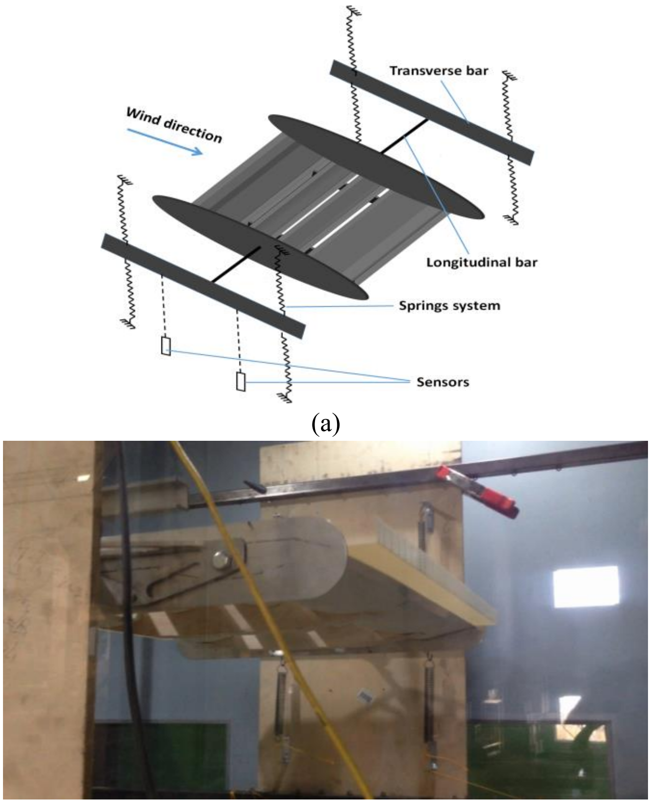

(a)

(b)

Fig. 4 Dynamic wind tunnel test (a) Schematic representation of the spring suspension system (b) Bridge deck setup for the wind tunnel dynamic test the tested bridge deck section model were calculated based on the free vibration test, and it was found that the natural frequency of the model in vertical direction was f_{h}=1.398 Hz, the natural frequency in torsional direction was f_{α}=1.982 Hz, the frequency ratio was $\varepsilon = f_{\alpha}/f_{\mathrm{h}} = 1.409$, the damping ratio in vertical direction was $\xi_{\mathrm{h}} = 0.0113$, and the damping ratio in torsional direction was $\xi_{\alpha} = 0.0132$.

3. Aerodynamic coefficients and vibration responses

Installing the windshields barriers on the four-box bridge deck model increased the drag coefficient for the positive angles of attack α = 0° to 6° (Fig. 5(a)), when compared with the same four-box deck with no windshields (Wang *et al*. 2015), however this was still significantly lower than the drag coefficients of Messina Bridge deck, composed of three box decks (Diana *et al*. 1995). The lowest drag coefficients were reported for Stonecutters Bridge twin deck, for both positive and negative angles of attack (Hui 2013). Meanwhile, the windshield barriers have the effect of decreasing the slope of the drag force coefficient, for the negative range of angles of attack, which is smoother when compared with the four-box bridge deck model without windshields barrier. The lift coefficients for the four-box deck model with windshields increased gradually with the increase of angle of attack from -6° to 6°, as it can be noticed in Fig. 5(b). Obviously, the installation of the windshield barriers decreased the lift coefficients for all angles of attack tested, maintaining however the same increasing evolution as for the lift coefficients reported for other multiple-decks sections (Wang *et al*. 2015, Diana *et al*. 1995) thus the slope was not affected. The twin-box decks stand apart from the multiple-box bridge decks, showing a wider variation of lift coefficients, as reported for Stonecutters Bridge (Hui 2013). A higher slope and a smaller range of magnitudes for the lift coefficient, and higher drag coefficients, have a stabilizing effect for the galloping instability as per Den Hartog criterion (Den Hartog 1956), especially in the positive range of angles of attack for the current four-box bridge deck.

$$H(\alpha) = \left(\frac{dC_L(\alpha_C)}{d\alpha_C} + C_D(\alpha_C) \right)\Bigg|_{\alpha_C=\alpha} < 0 \tag{3}$$

Verification of the Den Hartog expression for the lift and drag coefficients reported in Figs. 5(a) and 5(b) for the four-box bridge deck section, showed that galloping could be encountered for negative angles of attack, for which $H(\alpha)$ was determined to be in the range of -0.07 to -0.02. For angles of attack α = 0° to 6°, $H(\alpha)$ was positive, in the range of 0.0 to 0.13, thus showing that the proposed deck model would not encounter galloping instability. To verify experimentally the occurrence of this aerodynamic instability, the vertical and torsional vibrations of the four-box deck model were measured in the wind tunnel for the four-box bridge deck model suspended on the spring system, for angles of attack between -6 ° and +6°, and Re numbers of 0.48×10^5 to 6.66×10^5. The tests were performed

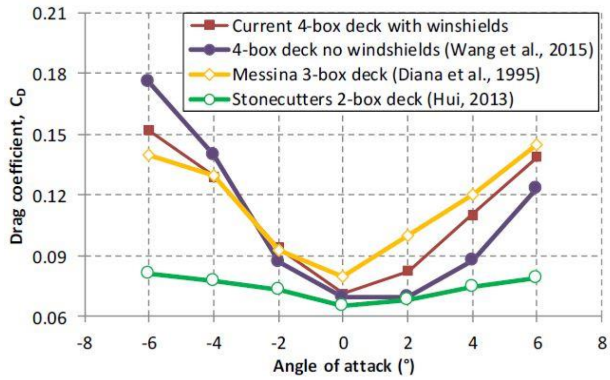

(a)

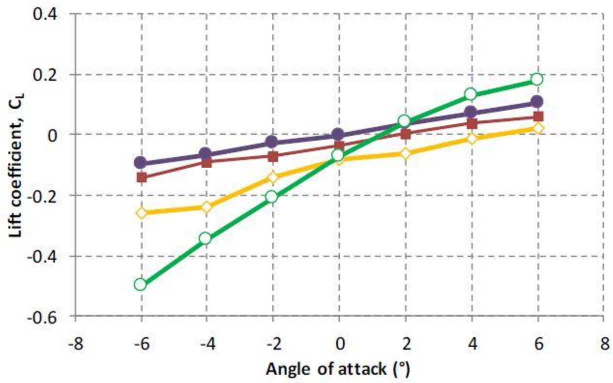

(b)

Fig. 5(a) Drag coefficient C_D and (b) Lift coefficient C_L for the four-box bridge deck with windshields of 30 mm and without windshields, at 8 m/s, 9 m/s and 10 m/s

in very small steps between *Re* 0.5 x 10^5 and 2 x 10^5 to detect the occurrence of the VIV response, while for higher *Re* numbers the galloping response was verified. The mean non-dimensional vertical amplitudes of vibration, *A/D*, where D is the width of the deck model, and torsional vibrations in radians represented in Figures 6 and 7, showed that the wind-induced responses increased with the wind speed, for both bridge deck models, Model 1 with 30 mm and Model 2 with 50 mm high windshields. For Model 1, at lower *Re* numbers, of up to 1.8×10^5, (test wind speed below 4.0 m/s), the magnitudes of both vertical and torsional vibrations were rather constant; however the response gradually increased with the increase of *Re* number, becoming considerably higher especially for -6° and +6° (Figs. 6(a) and 6(b)). A similar trend of increasing vertical and torsional vibrations for higher *Re* numbers was noticed for Model 2 (Figs 7(a) and 7(b)), however the difference between the responses recorded at -6° and +6°, and the other angles of attack of -4°, -2°, 0 +2° and +4°, was not as high as for the previous case. Overall the 50 mm high windshield model (Model 2) had similar response, for lower Re numbers of up to 1.8×10^5, recording vertical vibrations of up to $A/D = 2.0\times10^{-3}$ when compared with $A/D = 1.92\times10^{-3}$ for the Model 1 with 30 mm windshield. For higher *Re* numbers of 6.66×10^5, the maximum vertical response for the 50 mm windshield model was lower of up to $A/D = 11.43\times10^{-3}$, compared with $A/D = 13.2\times10^{-3}$, for the 30 mm windshield model. Similarly, for Model 2, the

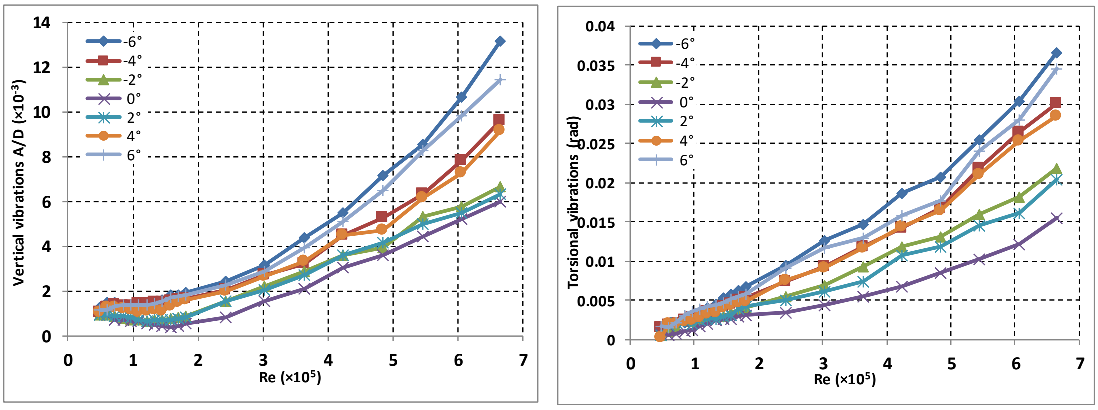

Fig. 6 Wind-induced response for Model 1 with 30 mm windshield model (a) Vertical vibrations (*A/D*) and (b) Torsional vibrations (rad)

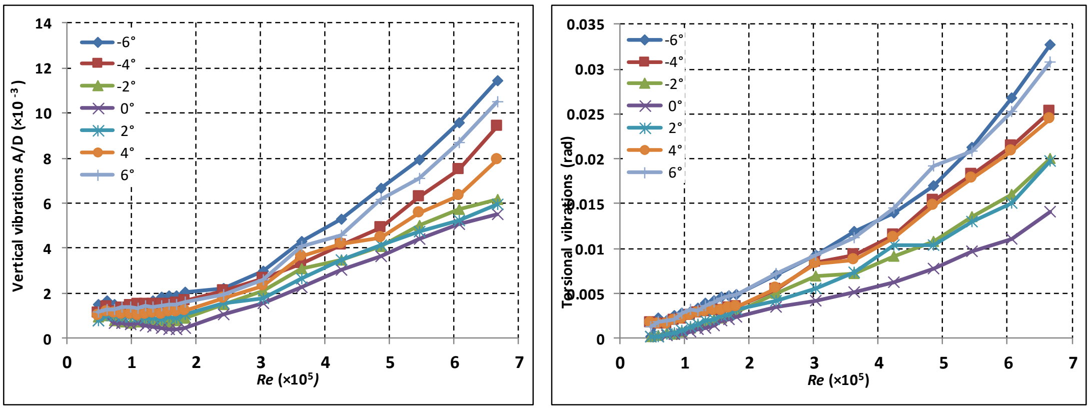

Fig. 7 Wind-induced response for Model 2 with 50 mm windshield model (a) Vertical vibrations (*A/D*) and (b) Torsional vibrations (rad)

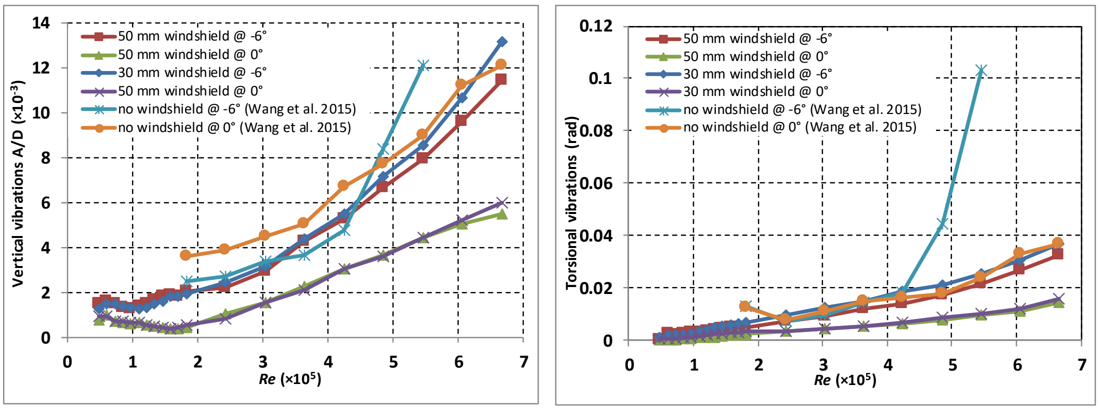

Fig. 8 Wind-induced response for four-box deck bridge deck model with windshields and without windshields, (a) Vertical vibrations (*A/D*) and b) Torsional vibrations (rad)

torsional response of up to 0.005 rad were recorded for lower *Re* of 1.8×10^5, while for higher *Re* numbers the torsional response increased up to 0.032 rad (Fig. 7(b)). For the Model 1, the torsional response was similar at lower *Re* numbers reaching 0.005 rad, and for higher *Re* numbers of 6.6×10^5 this gradually increased to a maximum value of 0.036 rad (Fig. 6(b)).

Also it could be noticed that, for both 30 mm and 50 mm windshields models, larger amplitudes for vertical and torsional vibrations were registered for negative angles of attack, thus the vibration amplitudes for -6° were higher than the response measured at +6°; similarly the responses for -4° and -2° were higher than the responses measured at +4° and +2° respectively. Always the wind-induced response recorded for 0° was the lowest. The study performed by Wang (2015) for a four-box bridge deck model without windshields revealed that vertical wind-induced responses at 0° were higher than the responses reported for the models with 30 mm and 50 mm windshields at 0°, for all wind speeds (Fig. 8(a)). For the case of -6° the vertical response was similar for the bridge deck models with windshields and without windshields for $Re = 4.2 \times 10^5$; a significant difference was noticed at higher Re, where the vertical and torsional responses of the four-box deck without windshields showed a sudden increase, indicating the occurrence of galloping (Wang 2015). The increase of wind-induced response is even more evident for the torsional vibrations for which the sudden increase was noticed from $Re = 5.0\times10^5$ (Fig. 8(b)). For the four-box bridge deck model with 30 mm and 50 mm windshields, the vertical and torsional responses gradually increased, but galloping did not occur for Re up to 6.6×10^5 (Figs. 8(a) and 8(b)). Thus, the 30 mm and 50 mm windshields installed on the bridge deck model, had the effect of decreasing the vertical and torsional vibrations, when compared with the model without windshield barriers, which obviously encountered aerodynamic instability for high wind speeds. The model with 50 mm high windshield barriers performed better than the model with 30 mm high windshield barriers, in mitigating the increase of both vertical and torsional vibrations. No VIV and galloping responses were detected for any of the tested models.

4. Flutter derivatives identification

Flutter derivatives are critical parameters for bridge flutter analysis, which can be directly extracted from the wind tunnel experiment results by employing a proper system identification method. Different methods for extraction of flutter derivatives can be used, however the aerodynamic self-excited forces for lift and moment formulations presented by Scanlan and Simiu, (1996), which include 16 flutter derivatives, are the most common for bridge design. The 16 flutter derivatives are H_i^* (K_h), H_i^* (K_α), A_i^* (K_h), and A_i^* (K_α), (i=1,2,3,4) as they appear in Eqs. 4 below. Among them, H_i^* (K_h) and H_i^* (K_α), (i=1,2,3,4) are used for calculating the aerodynamic lift force, L_{ae} and A_i^* (K_h), (i=1,2,3,4) are used for obtaining the aerodynamic moment M_{ae}. Iwamoto and Fujino (1995) investigated the effect of coupling between the bending and torsional motions of a bridge deck section model tested in wind tunnel, under smooth wind flow and they showed that the weak coupling between these motions can allow for a simplification of the terms containing α and $\dot{\alpha}$ related to the vertical frequency ω_h and the terms containing h and $\dot{h}$ related to the rotational frequency ω_α, which thus can be neglected. Therefore as a general approach, the 16 flutter derivatives are reduced to 8 flutter derivatives and the aerodynamic forces are formulated per unit length of deck as (Iwamoto and Fujino 1995):

$$\begin{aligned} L_{ae} &= \frac{1}{2}\rho U^2 B\left[K_h H_1^*\frac{\dot{h}}{U} + K_\alpha H_2^*\frac{B\dot{\alpha}}{U} + K_\alpha^2 H_3^*\alpha + K_h^2 H_4^*\frac{h}{B}\right] \\ M_{ae} &= \frac{1}{2}\rho U^2 B^2\left[K_h A_1^*\frac{\dot{h}}{U} + K_\alpha A_2^*\frac{B\dot{\alpha}}{U} + K_\alpha^2 A_3^*\alpha + K_h^2 A_4^*\frac{h}{B}\right] \end{aligned} \tag{4}$$

where, ω_h is the vertical bending frequency, ω_α is the torsional frequency, U is the mean wind speed, B is the width of the bridge deck (m), ρ is the air density (kg/m^3) and K is the reduced frequency. The flutter derivatives are H_1^*, H_4^*, A_2^*, and A_3^*, depend of ω_h, which means that these four flutter derivatives are related to the bending response and therefore these are called direct-flutter derivatives as they can be identified by analyzing a single-degree-of-freedom model system. Similarly, the other four flutter derivatives H_2^*, H_3^*, A_1^*, and A_4^*, can be obtained through the torsional responses (Sarkar 1992) and are characteristic to a two-degree-of-freedom system with the coupled motion, thus these can be obtained by investigating the motion of the other degrees-of-freedom. The flutter equation of motion of a two-degree-of-freedom bridge section model under smooth wind flow can be expressed in matrix form as (Simiu and Scanlan 1996):

$$[M][\ddot{X}] + [C][\dot{X}] + [K][X] = [F_{ae}] \tag{5}$$

Where the aeroelastic self-excited force F_{ae} can also be expressed as the matrix format as:

$$[F_{ae}] = \begin{bmatrix} L_{ae} \\ M_{ae} \end{bmatrix} = \begin{bmatrix} \frac{1}{2}\rho U^2 B & 0 \\ 0 & \frac{1}{2}\rho U^2 B \end{bmatrix} \begin{bmatrix} \frac{KH_1^*}{U} & \frac{KH_2^* B}{U} & K^2H_3^* & \frac{K^2H_4^*}{B} \\ \frac{KA_1^*}{U} & \frac{KA_2^* B}{U} & K^2A_3^* & \frac{K^2A_4^*}{B} \end{bmatrix} \begin{bmatrix} \dot{h} \\ \dot{\alpha} \\ h \\ \alpha \end{bmatrix} \tag{6}$$

Assigning the corresponding terms for the aeroelastic effective damping and stiffness matrices of the system, [C^{eff}] and [K^{eff}] respectively and for the mechanical damping and stiffness matrices [C^{mech}] and [K^{mech}] set under no wind speed condition, the expression formula for each flutter derivative can be obtained as:

$$\begin{aligned} H_1^*(K) &= -\frac{2m}{\rho B^2\omega_h}(C_{11}^{eff} - C_{11}^{mech}) & H_2^*(K) &= -\frac{2m}{\rho B^3\omega_\alpha}(C_{12}^{eff} - C_{12}^{mech}) \\ H_3^*(K) &= -\frac{2m}{\rho B^3\omega_\alpha^2}(K_{12}^{eff} - K_{12}^{mech}) & H_4^*(K) &= -\frac{2m}{\rho B^2\omega_h^2}(K_{11}^{eff} - K_{11}^{mech}) \\ A_1^*(K) &= -\frac{2I}{\rho B^3\omega_h}(C_{21}^{eff} - C_{21}^{mech}) & A_2^*(K) &= -\frac{2I}{\rho B^4\omega_\alpha}(C_{22}^{eff} - C_{22}^{mech}) \\ A_3^*(K) &= -\frac{2I}{\rho B^4\omega_\alpha^2}(K_{22}^{eff} - K_{22}^{mech}) & A_4^*(K) &= -\frac{2I}{\rho B^3\omega_h^2}(K_{21}^{eff} - K_{21}^{mech}) \end{aligned} \tag{7}$$

As Eq. (7) shows, the known parameters are, the mass of the model m (kg), the mass moment of inertia I, the circular natural frequency ω_h, ω_α, for bending and torsion motions, respectively. The only unknown parameters are the aeroelastic effective damping and stiffness matrices.

Currently several system identification methods exist for the unknown system parameters involved in a standard dynamic wind tunnel test, such as such as the Ibrahim Time Domain (ITD) method, the Modified Ibrahim Time Domain (MITD) method, the First-Order Reliability (FOR) method, Iterative Least Squares (ILS), (Chowdhury and Sarkar 2003, Yang *et al.* 2010, Mohanty and Rixen 2004, Ibrahim and Mikulcik 1977). Iterative least squares method was employed for the data measured in the current experiment, as described by Chowdhury and Sarkar (2003). A low-pass digital Butterworth filter was applied for eliminating the noise interferences from the recorded vibration time histories, for which the cut-off frequencies were selected based on the energy content of each measured data, determined by a Fast Fourier Transform. Once the filtered time histories were obtained, a Matlab code was written for applying the finite difference formulation to generate velocity and acceleration time histories as described by Chowdhury and Sarkar (2003). To minimize the filter and the finite difference altering effect on the recorded data, a “windowing” procedure was used by taking only the middle part of the three time histories for the construction of initial least square matrix of the displacements and velocities defined as:

$$A^0 = (X\dot{X}^T)(XX^T)^{-1} \tag{8}$$

Using the initial conditions X^0, the vibration time history X^1 was simulated for the next time step, as the exponential of the initial matrix A^0 and the residuals were recalculated considering the least square matrix estimated for the successive time steps. The convergence criteria for the matrix A was considered in the order of 10^{-6}.

$$X^1 = e^{A^0 t} X^0,\ \ A^1 = (X\dot{X}^{1^T})(XX^{1^T})^{-1} \tag{9}$$

$$R_{i,j} = abs(A^k_{i,j} - A^{k-1}_{i,j}),\quad for\ \ i = n+1, \ldots 2n,\ \text{and}\ j = 1, \ldots, 2n \tag{10}$$

4.1. Windshields effect on aerodynamic flutter derivatives

Figs 9 and 10 show the flutter derivatives for the four-boxes bridge deck models with 30 mm and 50 mm high windshields, for the angles of attack -6°, 6° and 0°, where the vertical and torsional vibrations were highest and lowest, respectively. The flutter derivatives for the other tested angles of attack were not included due to graphical visualisation comprehensibility. With the increase of the reduced wind speeds, the absolute values for all eight flutter derivatives had a general increasing trend, when positive values are encountered and a general decreasing trend for negative values. Among the eight flutter derivatives, H_2^*, H_4^* and A_4^* showed more variation along the general increment or decrement trends. Also considering that the H_1^* flutter derivative, which is related to the aerodynamic damping in the vertical direction, is negative, then flutter instability might occur for both models, 30 mm windshield bridge deck model and the 50 mm windshield model. The H_2^* flutter derivative, related to the torsional damping in the coupled motion, had a slight stagnation initially until reduced wind speed of $U/fB = 2.8$, after which this decreased gradually until maximum reduced wind speed of U/fB =9.8, except for the case of 50 mm windshield at 0°, where an increase was noticed between U/fB =2.66 and 4.5. This is a first indication that the 50 mm windshield model would perform better for torsional instability. H_3^*, corresponding to the lift force contribution from the torsional displacement, decreased steadily with the increase of the reduced wind speed, however for $U/fB =$ 6.2 and 7.1, the model with 50 mm windshield registered an increase for 0°. The model with 30 mm windshield is expected to encounter torsional instability, as from reduced wind speed of U/fB =7.1 to at $U/fB =$ 9.8, both flutter derivatives, H_3^* and H_2^* had a sudden decrease, for 0° angle of attack. For both windshields models, as expected, H_4^*, which represents the aerodynamic stiffness associated with the torsional motion, had a similar evolution as the H_2^* flutter derivative, but the increasing part for the range of $U/fB = 2.66$ to 4.5, was registered for all tested cases, except for the model with 30 mm windshield under 6° angle of attack, where a more constant decrease was noticed. However, H_4^*, does not significantly affect the overall flutter behaviour of the bridge (Scanlan and Tomoko 1971), thus many studies would report only the first six flutter derivatives.

Fig. 10 shows that for the A_1^* flutter derivative, which conveys the damping for the vertical vibration mode, measured for both models, 30 mm and 50 mm high windshields, the angle of attack did not increase significantly, when compared with the other flutter derivatives. A destabilizing effect for coupled flutter is expected when the absolute values of both flutter derivatives A_1^* and H_3^* increase, however in the current case the H_3^* was lower, especially for the model with 50 mm high windshields. A stabilizing effect is induced by the A_2^* flutter derivative, which represents the non-dimensional aerodynamic damping for torsional vibration, and considering the decreasing negative values recorded, it can be concluded that then the models are not prone to torsional flutter; this occurs when the flutter divergent response is achieved without coupling with the vertical vibration mode. Also, the windshields height did not have a significant effect on the flutter derivative A_2^*, the curves for each angle of attack being very close to each other, except for the case of 0° for which at reduced wind speeds higher than $U/fB = 5.33$, slightly higher flutter derivatives were noticed for the deck model with 50 mm windshield. The installation of the windshields did not affect the non-dimensional aerodynamic stiffness contribution for the torsional mode, thus a similar trend was noticed for the A_3^* flutter derivative, except that the models tested for 0° registered the highest response, for both models. Even though the most variation was noticed for A_4^* flutter derivative, this relates to the stiffness term in the vertical vibration mode and it is not considered to contain important information for the flutter response estimation. For reduced wind speeds higher than $U/fB = 2.66$, the A_4^* flutter derivative curves suddenly increased for the 50 mm and 30 mm windshields models tested at 6°, recording a local decrement at $U/fB = 5\ .33$ followed by a second increment for $U/fB = 7.2$, decreasing thereafter.

The experimental results of the flutter derivatives obtained for the current four-box bridge deck model with 30 mm and with 50 mm windshields were compared with the experimental results for the four-box bridge deck without any windshields, reported by Wang and Dragomirescu (2016), and with the results reported for other multi-box bridge deck models, such as Messina Bridge, which has a three-box bridge deck (Baldomir *et al*. 2013) and Stonecutters Bridge with a twin-box deck (Hui *et al*. 2013). As shown in previous studies (Rizzo *et al*. 2018) the flutter derivatives experimental results can register up to 3.3% of the sampled points outside the tolerance interval, thus the

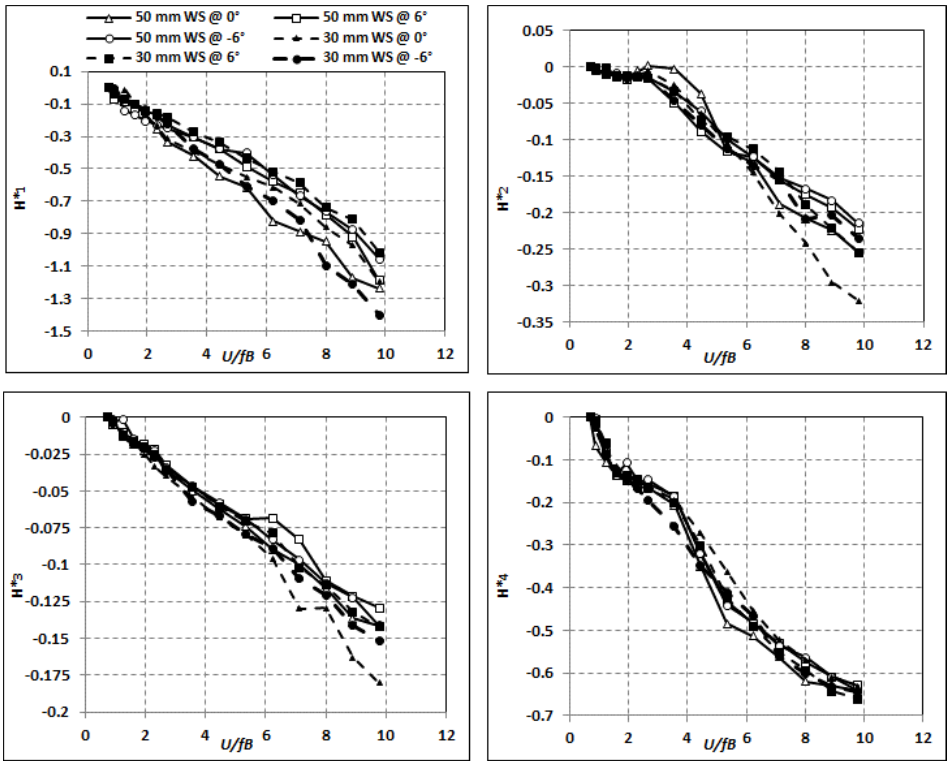

Fig. 9 Flutter derivatives for Model 1 (30 mm windshield) and Model 2 (50 mm windshield) for -6°, 0° and 6° angles of attack

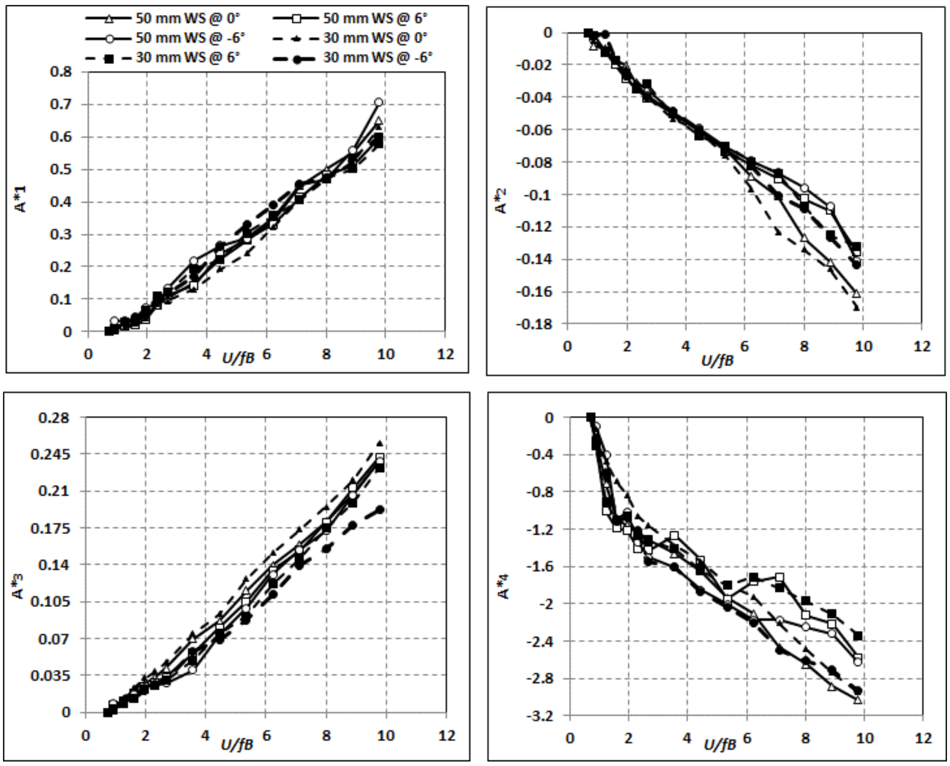

Fig. 10 Flutter derivatives for the Model 1 (30 mm windshield) and Model 2 (50 mm windshield) for -6°, 0° and 6° angles of attack

experimental error propagation can have a significant effect on measuring the flutter derivatives. For the current four-box deck models with 30 mm and 50 mm windshields, the flutter derivatives determined empirically did not exhibit high variation; however for the similar four-box deck, but without windshields (Wang and Dragomirescu 2016), the

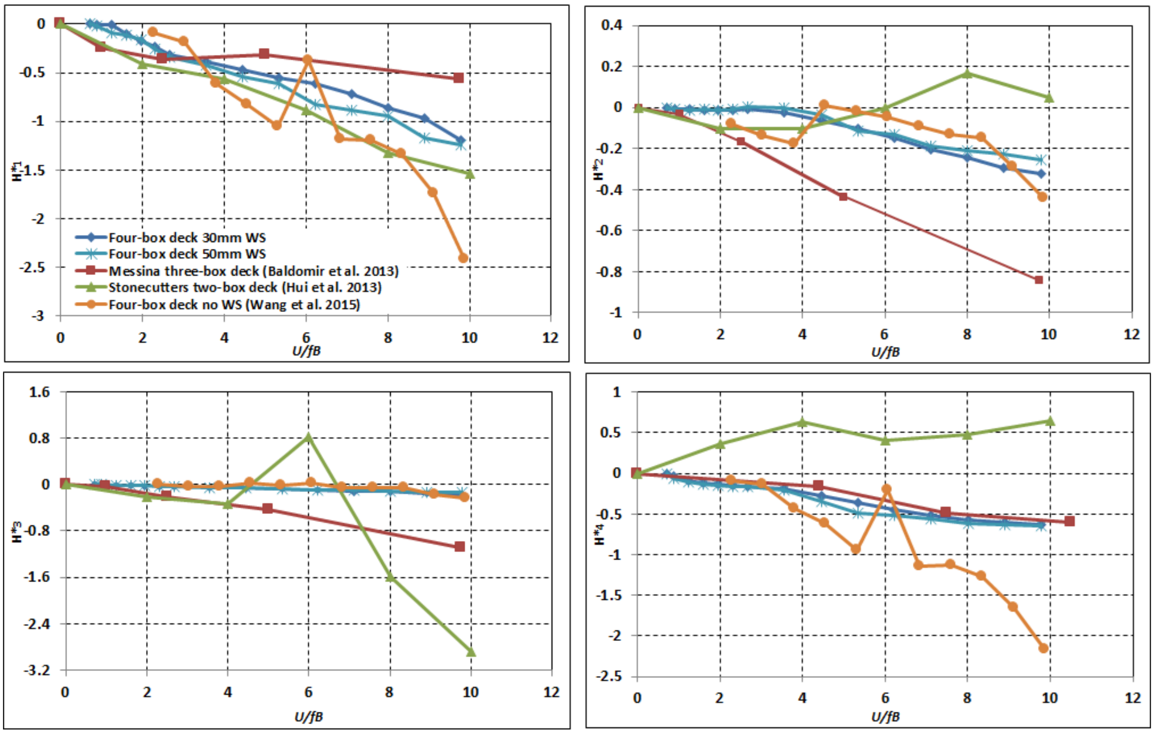

Fig. 11 Flutter derivatives comparison for different types of bridge decks models at 0° angle of attack

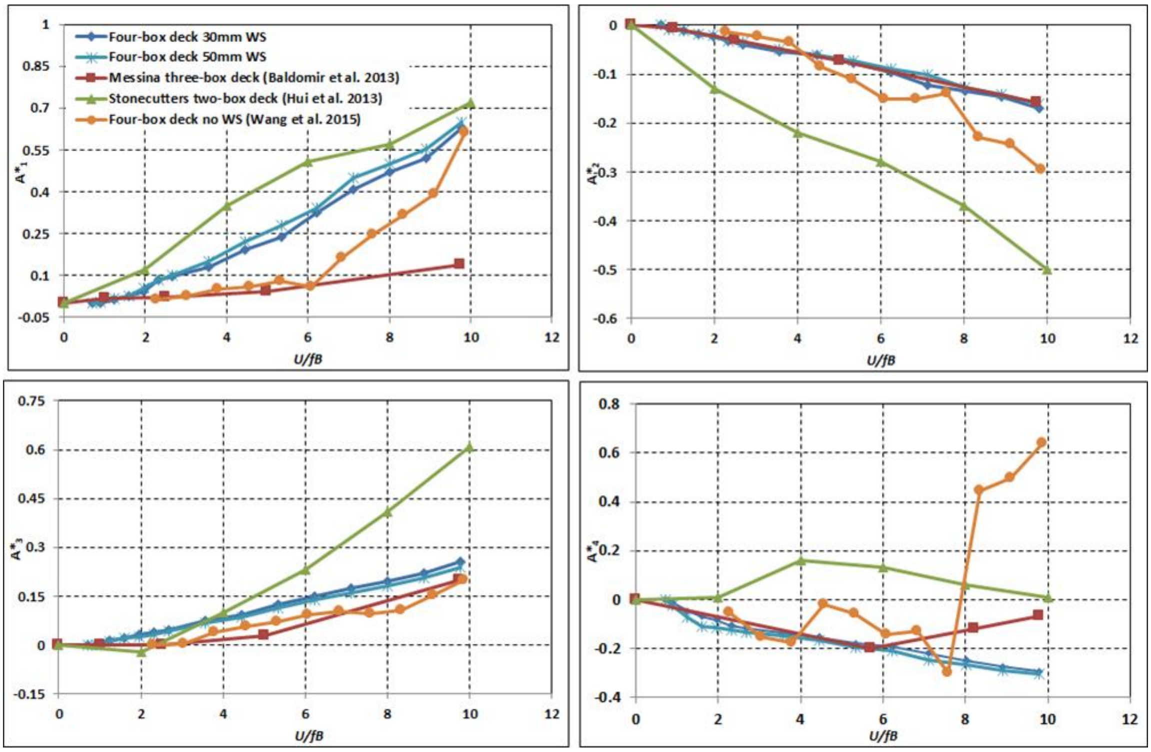

Fig. 12 Flutter derivatives comparison for different types of bridge decks models at 0° angle of attack

experimental data showed some discrepancies which can be attributed to the experimental measurements induced errors.

As it can be noticed in Figs 11 and 12, the H_2^*, A_2^* and A_3^* results, extracted from the experimental data of the four-box deck with 30 mm and 50 mm high windshields, agreed well with the experimental results obtained by Wang and Dragomirescu (2016) for the aerodynamic four-box deck without windshields. However, the flutter derivative A_4^* registered a significant discrepancy when compared with the results obtained from the four-box deck models with windshields, especially for reduced wind speeds higher than $U/fB = 7.6$. A similar discrepancy was noticed for H_1^* and H_4^*, for which the four-box deck model without windshields (Wang 2015) showed a local increment at

$U/fB = 6$, decreasing steadily afterwards. Thus, it was evident that using the windshields on the four-box bridge deck model, improved its aerodynamic performance.

Depending on the numbers of boxes composing the bridge deck models, the aerodynamic properties reflected by the flutter derivatives, had different evolution. Thus, for the direct-flutter derivatives, H_1^*, H_4^*, A_2^* and A_3^*, the four-box deck model showed good agreement with that of the Messina Strait Bridge deck. The H_1^* results reported for the twin-box Stonecutters Bridge deck, had some similarities with those of the four-box bridge deck and the three-box Messina Strait Bridge deck; the other flutter derivatives of the Stonecutters Bridge deck however, indicated large discrepancies when compared with the three-box and four-box bridge decks (Fig. 11(a)). Therefore, for the one-degree-of-freedom vibration motions, only the four-box girder bridge deck compared well with the three-box deck girder bridge of the Messina Strait Bridge, thus grouping them in a distinct category of multiple-box bridge decks. Due to the fact that the cross-flutter derivatives, H_2^*, H_3^*, A_1^* and A_4^* are obtained through coupled motion vibrations, these parameters would differ significantly among different types of bridge decks. For H_2^*, there is a considerable difference between the four kinds of bridge decks, the Stonecutters Bridge deck flutter derivative decreased initially, followed by a steady increase afterwards (Fig. 11(b)); the Messina Bridge deck decreased gradually until maximum reduced wind speed $U/fB = 10$, while the current four-box bridge deck had a more consistent evolution, registering only a limited decrease. The H_3^* flutter derivative, corresponding to the lift force resulted from the self-excited motion, for the multiple-box decks models, H_3^* presented the smallest variation among the eight flutter derivatives (Fig. 11(c)). The same flutter derivative H_3^* for the twin-box deck model of the Stonecutters Bridge however, decreased sharply after $U/fB = 6$. In comparison to the other H^* flutter derivatives, H_4^* had closer agreement between the four-box and three-box Messina bridge deck models, for all reduced wind speeds (Fig. 11(d)); therefore, changing the height of the edge windshield or extending the width of the deck with two more box decks, did not affect significantly the values of H_4^*. Similarly for A_2^* flutter derivative, an obvious conclusion was that different heights of the windshields did not have a major effect; also the four-box deck results agreed very well with the results reported by Baldomir *et al.* (2013) for Messina three-box deck (Fig. 12 (b)). For both A_2^* and H_4^*, installing the windshields on the four-box deck helped stabilizing the aerodynamic response of the model. For A_1^* flutter derivative, the four-box bridge deck model without windshields registered results very similar to the Messina three-bridge box deck, until $U/fB = 6$, increasing for higher reduced wind speeds (Fig. 12(a)). The four-box bridge deck models with 30 mm and 50 mm windshields registered A_1^* flutter derivative values consistent with each other, but had higher values than the other multiple-box bridge decks, and lower than the twin-box Stonecutters Bridge deck model.

The A_3^* flutter derivative, representing the effect of the uncoupled aerodynamic stiffness on the frequency and damping parameters, showed a lower variation for the three-box and four-box bridge decks, but registered higher values for the twin-box Stonecutters Bridge (Fig. 12(c)). The trends for the A_3^* flutter derivative for 30 mm and 50 mm windshield models were similar, but the four box-deck model without windshields compared better with the three-box Messina bridge deck. The flutter derivative A_4^* depends on the pitching moment component of the vertical motion in the two degrees of freedom system vibrations. The A_4^* trend lines presented in Figure 12 d) were different for each type of bridge deck model discussed: while the A_4^* values for the four-box bridge decks with 30 mm and 50 mm were consistent with each other, and gradually decreasing, the A_4^* values for the model without windshields registered a higher variation and a sudden increase from $U/fB = 7.6$. The Messina Bridge deck had a good agreement with the four-box bridge deck with windshields, until $U/fB = 6.0$, but increased steadily thereafter. The Stonecutters Bridge deck is the single deck model which has only positive values for the same flutter derivative, increasing until $U/fB = 4$, but decreasing gradually until almost 0 at $U/fB = 10$.

5. Conclusions

The effect of windshields barriers with 30 mm and 50 mm heights built for a four-box bridge deck model, was investigated through wind tunnel experiments and it was found that these have a significant effect on aerodynamic characteristics of the bridge deck. In general, it could be concluded that (1) at low reduced wind speeds, of up to $U/fB = 2.66$, for most of the flutter derivatives, there was no obvious effect of the angle of attack. (2) For reduced wind speeds higher than $U/fB = 2.66$, higher flutter derivatives were observed at 6° and -6°, especially for H_1^* and A_4^*. (3) The flutter derivatives obtained for both models, the four-bridge deck with 30 mm and with 50 mm windshields, were very similar, however for the A_4^* flutter derivative, the model with 50 mm windshield had a better performance.

Also, the cross-flutter derivatives experimentally obtained for the four-box bridge deck model with windshields and without windshields compared better with the Messina Bridge deck, except for A_4^*, where different responses were noticed for the three types of models beyond $U/fB = 6$. The direct flutter derivatives were more consistent for all the multiple-box bridge decks, except for H_1^*, for which the results for all the discussed bridge deck models showed more scatter. Finally, when comparing with other twin-box and triple-box bridge decks models, the effect of the windshields height of 30 mm or 50 mm for the four-box bridge deck model, was not dominant, however when comparing with the same four-box deck but without windshields, it was evident, that these improve the aerodynamic stability of the entire deck. The windshield porosity and the effect of the incoming turbulent wind are important parameters, which influence the aerodynamic characteristics of a bridge deck, thus these will be tested in a second phase of the experimental investigation.

Acknowledgments

This research was supported through the NSERC Discovery grant number 145278 - 06776. Also the authors are grateful to Dr. Muslim for the advices and assistance when preparing the experiments, Dr. Bas Baskaran and Dr. Steve Ko, who lend some of the equipment needed for the experiment. Particularly the authors would like to acknowledge the support of Mr. Vicent Ferraro, Mr. Dave Menard and Mr. Ryan Rosborough from Gradient Wind Engineering, for modifying the experimental model and for making their wind tunnel available for this research project.

References

Baldomir, A., Kusano, I., Hernandez, S. and Jurado, J.A. (2013), "A reliability study for the Messina Bridge with respect to flutter phenomena considering uncertainties in experimental and numerical data", *Comput. Struct*., **128**, 91-100. https://doi.org/10.1016/j.compstruc.2013.07.004.

Buljac A., Kozmar H., Pospísil S. and Machacek M. (2017), "Flutter and galloping of cable-supported bridges with porous wind barriers", *J. Wind Eng. Ind. Aerod.*, **171**, 304-318. https://doi.org/10.1016/j.jweia.2017.10.012.

Chen N., Li N., Wang B., Su Y. and Xiang H. (2015), "Effects of wind barrier on the safety of vehicles driven on bridges", *J. Wind Eng. Ind. Aerod.*, **143**, 113-127. https://doi.org/10.1016/j.jweia.2015.04.021.

Chowdhury, A.G. and Sarkar, P. (2003), "A new technique for identification of eighteen flutter derivatives using a *three-*degree-of-freedom section model", *Eng. Struct.*, **2**(14), 1763-1772. https://doi.org/10.1016/j.engstruct.2003.07.002.

Diana, G., Falco, M., Bruni, S., Cigada, A., Larose, G.L., Damsgaard, A and Collina, A. (1995), "Comparisons between wind tunnel tests on a full aeroelastic model of the proposed bridge over Stretto di Messina and numerical results", *J. Wind Eng. Ind. Aerod.*, **54-55**, 101-113. https://doi.org/10.1016/0167-6105(94)00034-B.

Dragomirescu E., Wang Z. and Hoftyzer M.S. (2016), "Aerodynamic characteristics investigation of Megane multi-box bridge deck by CFD-LES simulations and experimental tests", *Wind Struct*., **22**(2), 161-184. https://doi.org/10.12989/was.2016.22.2.161.

Den Hartog J.P. (1956), "Mechanical Vibrations", McGraw Hill, New York.

Hui, C.H.M. (2013), "Full-bridge aero-elastic model wind tunnel tests for the Stonecutters Bridge", *HKIE Transactions*, **20**(2), 109-123. https://doi.org/10.1080/1023697X.2013.794554.

Ge, Y.J. and Xiang, H.F. (2009), "Aerodynamic stabilization for box-girder suspension bridges with super-long span", *The Proceedings of the 5th EACWE*, Florence, July.

Ibrahim, S.R. and Mikulcik, E.C. (1977), "A method for direct identification of vibration parameters from the free response", *Shock Vib. Bull.*, **47**(4), 183-198.

Iwamoto, M and Fujino, Y. (1995), "Identification of flutter derivatives of bridge deck from free vibration data", *J. Wind Eng. Ind. Aerod*., **54-55**, 55-63. https://doi.org/10.1016/0167-6105(94)00029-D.

Kozmar H., Procino L., Borsani A. and Bartoli G. (2012), "Sheltering efficiency of wind barriers on bridges", *J. Wind Eng. Ind. Aerod.*, **107-108**, 274-284. https://doi.org/10.1016/j.jweia.2012.04.027.

Kwon S., Kim, D., Lee, S. and Song, H. (2011), "Design criteria of wind barriers for traffic (Part 1: wind barrier performance)", *Wind Struct.*, **14**(1), 55-70.

Lin, T.Y. and Chow, P. (1991), "Gibraltar Strait Crossing, a challenge to bridge and structural engineering", *IABSE J. Struct. Eng*., 1(2). https://doi.org/10.2749/101686691780617779.

Lee, M., Kim, S. and Seo Y. (2012), "The Yi Sun-sin Bridge: Innovative Solutions for Suspension Bridges", *Struct. Eng. Intl*., **22**(1), 32-35. https://doi.org/10.2749/101686612X13216060213158.

Meng, X. (2013), "Study on the windbreak performance of wind barrier on the long-span bridge", Master Thesis, Beijing Jiaotong Universtity, China.

Mohanty, P. and Rixen D.J. (2004), "A modified Ibrahim time domain algorithm for operational modal analysis including harmonic excitation", *J. Sound Vib*., 275(1-2), 375-390. https://doi.org/10.1016/j.jsv.2003.06.030.

Morgenthal, G., Sham, R. and West. B. (2010), "Engineering the tower and main span construction of Stonecutters Bridge", *J. Bridge Eng.*, 15(2). https://doi.org/10.1061/(ASCE)BE.1943-5592.0000042.

Nieto, F., Hernández, S., Kusano, I. and Jurado, J.A. (2012), "CFD aerodynamic assessment of deck alternatives for a cable-stayed bridge", *The Seventh International Colloquium on Bluff Body Aerodynamics and Applications (BBAA7)*, Shanghai, China, September.

Procino L., Kozmar H., Bartoli G and Borsani A. (2008), "Wind barriers on bridges: the effect of wall porosity", *The Sixth International Colloquium on Bluff Body Aerodynamics and Applications (BBAA6)*, Milano, Italy, July.

Rizzo F., Caracoglia L. and Montelpare S. (2018), "Predicting the flutter speed of a pedestrian suspension bridge through examination of laboratory experimental errors", *Eng. Struct*., **172**, 589-613. https://doi.org/10.1016/j.engstruct.2018.06.042.

Simiu, E. and Scanlan, R.H. (1996), "Wind Effect on Structures", John Wiley & Sons, Inc. New York, New York, U.S.A.

Sarkar, P. (1992), "New identification methods applied to the response of flexible bridges to wind", *Ph. D. Dissertation*, The John Hopkins University, Baltimore, U.S.A.

Scanlan, R.H. and Tomoko J.J. (1971), "Airfoil and bridge deck flutter derivatives," *J. Eng. Mech.*, **97**, 1717-1737.

Štrukelj, A., Ciglarič, I. and Pipenbaher, M. (2005), "Analysis of a bridge structure and its wind barrier under wind loads", *IABSE Struct. Eng. Intl.*, **15**(4), 220-227. https://doi.org/10.2749/101686605777962883.

Wang Z. and Dragomirescu E. (2016), "Flutter derivatives identification and aerodynamic performance of an optimized multibox bridge deck", *Advan. Civil Eng*., **2016**, 8530154. https://doi.org/10.1155/2016/8530154.

Wang, Z. (2015), "Experimental and CFD investigations of the Megane multi-box bridge deck aerodynamic characteristics", *Master Thesis*, Civil Engineering Department, University of Ottawa, Canada.

Wangsadinata, W. (1997), "The Sunda Strait Bridge and its feasibility as a link between Jawa and Sumatera", *Report to BPP Teknologi*, Jakarta.

Yang, Z., Zhang, L., Liu, H. and Zhang, J. (2010), "Optimization of extracting flutter derivative based on Modified Ibrahim Time Domain method", *J. Civil Architect. Environ. Eng.*, 32(2).

AD